Control of Fixed-Wing Tethered Aircraft in Circular Take-Off and Landing Maneuvers

Sérgio Vinha[a], Gabriel M. Fernandes[b], Manuel C. R. M. Fernandes[c], Huu Thien Nguyen[d] and Fernando A. C. C. Fontes[e]

SYSTEC-ISR-ARISE, Department of Electrical and Computer Engineering, Faculty of Engineering, University of Porto, Rua Dr. Roberto Frias, 4200-465 Porto, Portugal

Keywords: Airplane Control, Tethered Aircraft, Automatic Take-off and Landing, Circular Take-off and Landing, Unmanned Aerial Vehicles (UAVs), Airborne Wind Energy.

Abstract: This article addresses the control of tethered aircraft with fixed wings during take-off and landing maneuvers with a circular motion, particularly focusing on controlling the aircraft's roll attitude. The tether forces acting on the aircraft make the roll control, in some operating regions, particularly challenging or even impossible when just ailerons are used. We describe a novel bridle system to actuate on the roll angle, the development of a controller for such a device, and its integration in the overall take-off and landing control architecture. Simulation results are reported, showing the adequacy of the approach. Further analysis identifies operational regions where it is possible to have a tethered flight or a coordinated turn flight as a function of the tether length and of the aircraft's height.

1 INTRODUCTION

In the last few years, we have been witnessing a rapid increase in tethered aircraft applications and in the literature on this subject. A recent survey (Marques et al., 2023) identified a broad range of applications, namely inspection/monitoring, security/surveillance, military, agricultural spraying, communications, vehicle towing and the generation of electrical power. The latter application, known as Airborne Wind Energy (AWE), has seen a particularly active research (Schmehl, 2018; Directorate-General for Research and Innovation (European Commission) and Ecorys, 2018).

Airborne Wind Energy Systems (AWES) are mechanisms that convert wind energy into electricity using autonomous aircraft attached to the ground by a tether. These mechanisms can harvest wind energy at high altitudes, where the wind is stronger and less intermittent, being able to generate electricity from a yet unexplored renewable energy resource. This makes AWE a promising renewable energy player. However, developing AWES into a competitive and commercially viable renewable energy technology is challenging. One of the main challenges is the ability to operate safely, reliably, and autonomously for long periods of time in various weather and environmental conditions (see e.g., the European Commission report (Directorate-General for Research and Innovation (European Commission) and Ecorys, 2018) and a study for Airborne Wind Europe (Blanch et al., 2022)). Despite the progress made in this field, most existing technology demonstrators still require supervised operation, particularly in the take-off and landing phases, and thus, are not fully autonomous. To achieve full autonomous operation it is essential to develop reliable automatic Take-Off and Landing (TOL) schemes for tethered aircraft.

The control of tethered aircraft, in particular for AWE, is a demanding problem, but one for which a significant number of contributions has been produced (see e.g.(Vermillion et al., 2021) and the many references therein). Different Automatic Take-Off and Landing (ATOL) approaches for tethered aircraft have been tried (Fagiano and Schnez, 2017). Among those, we can distinguish three techniques for fixed-wing aircraft: linear, vertical and circular TOL techniques. In vertical TOL, the technology is vastly stud-

[a] https://orcid.org/0000-0002-6364-6736
[b] https://orcid.org/0009-0005-6321-8677
[c] https://orcid.org/0000-0003-2322-8182
[d] https://orcid.org/0000-0002-2266-9560
[e] https://orcid.org/0000-0003-3516-5094

Vinha, S., Fernandes, G., Fernandes, M., Nguyen, H. and Fontes, F.
Control of Fixed-Wing Tethered Aircraft in Circular Take-Off and Landing Maneuvers.
DOI: 10.5220/0013067000003822

In *Proceedings of the 21st International Conference on Informatics in Control, Automation and Robotics (ICINCO 2024) - Volume 2*, pages 319-326
ISBN: 978-989-758-717-7; ISSN: 2184-2809

ied in the multicopter area. The same happens in the linear TOL with the common airplanes. However, circular TOL has a much lower possibility of reusing existing similar technology and thus is the least investigated technique of the three. The Circular Take-off and Landing (CTOL) is the technique studied in this article and it has several advantages: the facility to re-launch due to the infinite runway (the aircraft can do as many turns as needed) and the low peak power and additional mass required for climbing (Vinha et al., 2024a). There are two variants of the CTOL technique. One of such variants, the most investigated one, uses a rotating platform or rigid arm to generate enough airspeed (Sieberling et al., 2011; Zanon et al., 2013; Geebelen et al., 2013; Rieck et al., 2017). Other variants use a tethered aircraft equipped with landing gear and propellers to produce the circular motion during the take-off and landing phases, similarly to the scheme studied here and in (Cherubini et al., 2017; Cherubini, 2017; Fernandes, 2023; Vinha et al., 2024b). It is also noteworthy that Miles Loyd, a pioneer of Airborne Wind Energy, describes in its seminal patent (Loyd, 1981) a mechanism based on a circular launch system.

A control system for automatic circular take-off and landing and transition to flight has been proposed, which can be adopted by a fixed-wing, self-motorized, tethered aircraft. The main application foreseen for the proposed technology is to include it in an Airborne Wind Energy System. It used a hierarchical control architecture. In the top layer, a supervisory controller is responsible for governing the transition between flight phases, for path-planning, and for setting the references to the lower-level controllers at each phase of operation. At the lower level, the controllers that were designed for each phase range from simple PID, controlling on a single variable, to multivariable optimal regulators for the locally linearized systems. This control architecture was detailed in (Vinha et al., 2024b) and is summarized here for completeness.

In this paper, we introduce a novel bridle actuator to control the angle between the wings and the tether and thereby control the roll angle of the tethered aircraft. We also develop a dynamic model and control system for the aircraft's roll angle, integrated into the overall control architecture.

The control of the roll angle in tethered aircraft can be demanding in some situations due to the tendency of the tether tension to impose a specific wings-tether angle. The take-off, landing, and transition to normal tethered flight are some of such demanding situations for which it is crucial to have a roll angle control authority. Here, we explore in the examples the roll control during the phase immediately after the take-off, in loiter with levelled wings, and in coordinated turn situations. The developed controllers have been tested in simulations. The results show the viability of the approach to take-off and transition to other tethered flight modes. In the analysis of the results, we identify viable operational regions according to tether length and height for different roll angle intervals.

The document is organized as follows. In Section 2, we derive the model used to represent the motion of a tethered aircraft and introduce the control architecture used. Next, in Section 3 we detail the parameters and results from simulations designed to test the proposed control system. Finally, in Section 4, we discuss the results and implications of the simulations, including a discussion of the conditions in which coordinated turn flight is possible.

2 TETHERED AIRCRAFT MODEL

The motion of a tethered aircraft, when the tether is taut, is constrained to the surface of a sphere with a radius equal to the tether length. Therefore, it is convenient to use spherical coordinates centred at the tether anchorage point. The aircraft's location is represented by (r, φ, β), where r is the radial distance, φ is the azimuth angle, and β the elevation angle (measured from the horizontal plane). The coordinate basis is denoted by $(\mathbf{e}_r, \mathbf{e}_\varphi, \mathbf{e}_\beta)$. See nomenclature in Table 1. In spherical coordinates, the position, velocity, and acceleration vectors are (Riley et al., 2006):

$$\mathbf{p} = \begin{bmatrix} r \\ \varphi \\ \beta \end{bmatrix}, \quad \dot{\mathbf{p}} = \begin{bmatrix} \dot{r} \\ r\cos\beta\,\dot{\varphi} \\ r\dot{\beta} \end{bmatrix}, \text{ and} \tag{1}$$

$$\ddot{\mathbf{p}} = \begin{bmatrix} \ddot{r} \\ r\cos\beta\,\ddot{\varphi} \\ r\ddot{\beta} \end{bmatrix} + \begin{bmatrix} -r\dot{\beta}^2 - r\dot{\varphi}^2\cos^2\beta \\ 2\dot{r}\dot{\varphi}\cos\beta - 2r\dot{\varphi}\dot{\beta}\sin\beta \\ 2\dot{r}\dot{\beta} + r\dot{\varphi}^2\cos\beta\sin\beta \end{bmatrix}. \tag{2}$$

The aircraft's velocity vector is also denoted by $\mathbf{V}$ ($\mathbf{V} = \dot{\mathbf{p}}$) and the airspeed vector is given by $\mathbf{V}_a = \mathbf{V} - \mathbf{V}_w$ where $\mathbf{V}_w$ is the wind speed vector (assumed zero in this work). The last term in $\ddot{\mathbf{p}}$ is due to the use of a rotating frame and is equal to $-\mathbf{F}_\mathrm{i}/m$, where $\mathbf{F}_\mathrm{i}$ represents the inertial force,

$$F_\mathrm{i} = m \begin{bmatrix} r\dot{\beta}^2 + r\dot{\varphi}^2\cos^2\beta \\ -2\dot{r}\dot{\varphi}\cos\beta + 2r\dot{\varphi}\dot{\beta}\sin\beta \\ -2\dot{r}\dot{\beta} - r\dot{\varphi}^2\cos\beta\sin\beta \end{bmatrix}. \tag{3}$$

It is also convenient to consider the body coordinate frame with basis $(\mathbf{e}_X, \mathbf{e}_Y, \mathbf{e}_Z)$, where $\mathbf{e}_X$ is the air-

Table 1: Nomenclature.

A	wing area $\left[\mathrm{m}^2\right]$
b	wingspan [m]
$c_\mathrm{D}, c_\mathrm{L}$	aerodynamic drag and lift coefficients
$\mathbf{F}_\mathrm{D}, F_\mathrm{D}$	aerodynamic drag vector and magnitude [N]
$\mathbf{F}_\mathrm{L}, F_\mathrm{L}$	aerodynamic lift vector and magnitude [N]
$\mathbf{F}_\mathrm{p}, F_\mathrm{p}$	propeller thrust vector and magnitude [N]
$\mathbf{F}_\mathrm{i}, F_\mathrm{i}$	inertial force vector and magnitude in a rotating frame [N]
$\mathbf{F}_\mathrm{t}, F_\mathrm{t}$	tether force vector and magnitude [N]
g	gravitational acceleration $\left[\mathrm{m\,s}^{-2}\right]$
m	mass [kg]
ρ	air density $\left[\mathrm{kg\,m}^{-3}\right]$
h	height [m]
$\mathbf{p}$	kite position
$\mathbf{V}, V$	kite velocity vector and magnitude $\left[\mathrm{m\,s}^{-1}\right]$
$\mathbf{V_a}, V_a$	kite airspeed vector and magnitude $\left[\mathrm{m\,s}^{-1}\right]$
$\mathbf{V_w}, V_w$	wind velocity vector and magnitude $\left[\mathrm{m\,s}^{-1}\right]$
$\mathbf{X}, \mathbf{U}$	state and control vectors
r, φ, β	spherical coordinates [m],[°, rad],[°, rad]
α, γ	angle-of-attack and flight-path angle [°, rad]
ϕ, θ, ψ	roll, pitch and yaw angles [°, rad]
ζ	wings-tether angle [°, rad]
$\omega_p, \omega_q, \omega_r$	roll, pitch and yaw rates $\left[^\circ\,\mathrm{s}^{-1}, \mathrm{rad\,s}^{-1}\right]$

craft's longitudinal axis pointing to its nose, $\mathbf{e}_Y$ is the transversal axis pointing out of the right wing, and $\mathbf{e}_Z$ is the aircraft's vertical axis pointing down from its belly.

We define also a set of angles that characterize the aircraft's attitude. The pitch angle, denoted by θ, is the angle between the direction of the aircraft's longitudinal axis $\mathbf{e}_X$ and the horizontal plane. The flight-path angle, denoted by γ, is the angle between the horizontal plane and the aircraft's velocity vector $\mathbf{V}$. The aircraft's angle-of-attack, denoted by α, is the angle between the aircraft's longitudinal axis and its velocity vector (when both the sideslip angle and the wind speed are considered to be zero, as is the case in this work). These three angles are represented in Fig. 1 and are related by the equation $\theta = \gamma + \alpha$. The roll angle, denoted by ϕ, is the angle between the horizontal plane and the aircraft's transversal axis $\mathbf{e}_Y$. We define also the wings-tether angle ζ to be the angle between the aircraft's transversal axis $\mathbf{e}_Y$ and the tether direction $\mathbf{e}_r$. These angles are related by the equation $\beta = \phi + \zeta$ and are represented in Fig. 2.

In the spherical coordinate frame, the kinematic

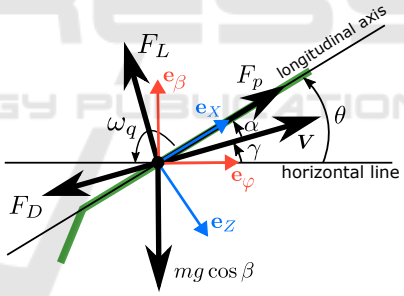

Figure 1: Airplane longitudinal model for circular tethered flight (aircraft longitudinal shape colored green).

model of the aircraft is

$$\begin{aligned} r\cos\beta\,\dot{\varphi} &= V\cos\gamma, \\ r\dot{\beta} &= V\sin\gamma, \\ \dot{\theta} &= \omega_q, \end{aligned} \tag{4}$$

where ω_q is the pitch rate. Taking the derivative of the kinematics (4), when r is assumed constant, we have

$$\begin{aligned} r\ddot{\beta} &= \sin\gamma\dot{V} + V\cos\gamma\dot{\gamma}, \\ r\cos\beta\,\ddot{\varphi} &= \cos\gamma\dot{V} - V\sin\gamma\dot{\gamma} \\ &\quad + \frac{V^2}{r}\tan\beta\cos\gamma\sin\gamma. \end{aligned} \tag{5}$$

The aircraft is subject to the following forces: the propeller thrust $\mathbf{F}_\mathrm{p} = F_\mathrm{p}\mathbf{e}_X$, the weight $\mathbf{F}_g$ with magnitude

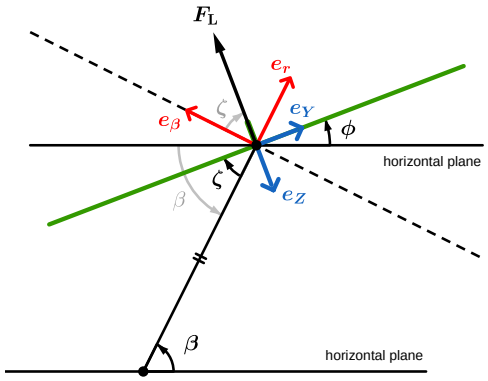

Figure 2: Tethered aircraft with wings-tether angle ζ possibly nonzero (aircraft lateral axis colored green).

mg pointing down, the aerodynamic lift $\mathbf{F}_\mathrm{L} = -F_\mathrm{L}\,\mathbf{e}_Z$, the aerodynamic drag $\mathbf{F}_\mathrm{D} = -F_\mathrm{D}\,\mathbf{e}_X$, the tether pull $\mathbf{F}_\mathrm{t} = -F_\mathrm{t}\,\mathbf{e}_r$, and also the inertial forces $\mathbf{F}_\mathrm{i}$ when a rotating frame are considered. In this setting,

$$F_\mathrm{D} = \frac{1}{2}\rho A {V_a}^2 c_\mathrm{D}(\alpha) \tag{6}$$

$$F_\mathrm{L} = \frac{1}{2}\rho A {V_a}^2 c_\mathrm{L}(\alpha) \tag{7}$$

where V_a is the magnitude of the airspeed vector $\mathbf{V}_a$.

Considering the total force in spherical coordinates $m\ddot{\mathbf{p}} = [F_r\, F_\varphi\, F_\beta]^\mathrm{T} = \mathbf{F}_\mathrm{L} + \mathbf{F}_\mathrm{D} + \mathbf{F}_\mathrm{p} + \mathbf{F}_\mathrm{g} + \mathbf{F}_\mathrm{t} + \mathbf{F}_\mathrm{i}$, we obtain for each component

$$\begin{aligned}
F_r =& F_\mathrm{L}\sin\zeta - F_\mathrm{t} - mg\sin\beta \\
&+ mr\dot{\beta}^2 + mr\dot{\varphi}^2\cos^2\beta, \\
F_\varphi =& -F_\mathrm{L}\sin\gamma\cos\zeta - F_\mathrm{D}\cos\gamma + F_\mathrm{p}\cos\theta \\
&- 2m\dot{r}\dot{\varphi}\cos\beta + 2mr\dot{\varphi}\dot{\beta}\sin\beta, \\
F_\beta =& F_\mathrm{L}\cos\gamma\cos\zeta - F_\mathrm{D}\sin\gamma + F_\mathrm{p}\sin\theta - mg\cos\beta \\
&- mr\dot{\varphi}^2\cos\beta\sin\beta - 2m\dot{r}\dot{\beta}.
\end{aligned} \tag{8}$$

Combining the last two equations with (5) and solving for $(\dot{V}, \dot{\gamma})$, we have

$$\begin{bmatrix} \sin\gamma & V\cos\gamma \\ \cos\gamma & -V\sin\gamma \end{bmatrix} \begin{bmatrix} \dot{V} \\ \dot{\gamma} \end{bmatrix} = \begin{bmatrix} F_\beta/m \\ F_\varphi/m - \frac{V^2}{r}\tan\beta\cos\gamma\sin\gamma \end{bmatrix},$$

which results in the dynamic equations for V and γ:

$$\begin{aligned}
m\dot{V} =& -F_\mathrm{D} + F_\mathrm{p}\cos\alpha - mg\cos\beta\sin\gamma - \frac{2V\dot{r}}{r}, \\
mV\dot{\gamma} =& F_\mathrm{L}\cos(\beta-\phi) + F_\mathrm{p}\sin\alpha - mg\cos\beta\cos\gamma \\
&- \frac{mV^2}{r}\tan\beta\cos\gamma.
\end{aligned} \tag{9}$$

These latter equations combine with the kinematics (4) to define the longitudinal motion model of the tethered aircraft. The resulting model is analogous to the well-known longitudinal model of a fixed-wing plane (see (Nguyen et al., 2023; Beard and McLain, 2012) and Fig. 1) when applied to the case of circular tethered flight.

We define the control variables to be the thrust force F_p, the pitch rate ω_q, and the wings-tether angle ζ.

The resulting state and control vectors considered are, respectively, $\mathbf{X} = [\varphi, \beta, V, \gamma, \theta]^\top$, $\mathbf{U} = [F_\mathrm{p}, \omega_q, \zeta]^\top$, and the state-space model is given by

$$\dot{\mathbf{X}} = f(\mathbf{X}, \mathbf{U}), \tag{10}$$

where the dynamic function f is obtained by combining equations (4) and (9), yielding

$$\begin{bmatrix} \dot{\varphi} \\ \dot{\beta} \\ \dot{V} \\ \dot{\gamma} \\ \dot{\theta} \end{bmatrix} = \begin{bmatrix} \frac{1}{r\cos(\beta)} V\cos\gamma \\ \frac{1}{r} V\sin\gamma \\ \frac{1}{m}\left[-F_\mathrm{D} + F_\mathrm{p}\cos\alpha - mg\cos\beta\sin\gamma\right] \\ \frac{1}{mV}\left[F_\mathrm{L}\cos\zeta + F_\mathrm{p}\sin\alpha - mg\cos\beta\cos\gamma \right. \\ \left. - \left(\frac{mV^2}{r}\right)\tan\beta\cos\gamma\right] \\ \omega_q \end{bmatrix}$$

2.1 Supervisory Controller

The control of a tethered airplane during the different stages of take-off, tethered flight and landing has various control requirements, needing different control references and even methodologies. As such, we have developed a hierarchical control architecture where, in the top layer, we have designed a supervisory controller that is responsible for overseeing phase transitions, path planning, and establishing references for lower-level controllers throughout each operational phase. Figure 3 delineates the operational phases considered. The operational phase follows closely the work (Vinha et al., 2024b), where further details can be found. In the current work, we will focus on the loiter phases and roll control (see Fig. 3, dashed and shadowed loiter phase). As explained below, we study three different loiter phases with distinct roll angles: (i) loiter with zero wings-tether angle, (ii) loiter with zero roll angle, and finally (iii) loiter with zero lateral acceleration in coordinated turn flight.

2.2 Roll Control and Wings-Tether Angle Actuation

In tethered aircraft, the tether tension tends to set the roll angle into a specific position, being very hard to drive to any other position just using the ailerons as in standard untethered airplanes. This is because the tether is restricting the motion and centrifugal forces play a major role in this situation. Therefore the aircraft's center of mass tends to align with the tether

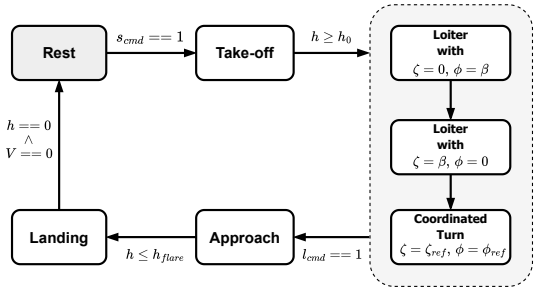

Figure 3: The different operational phases of a tethered aircraft during take-off and landing and three loiter maneuvers with three different roll angles ϕ (and the corresponding different wings-tether angles ζ).

direction. The roll position is $\phi = \beta$ if the tether attachment point is at the wing tip, or is $\phi = \beta - \pi/2$ if the attachment point is on the fuselage surface, on the vertical symmetry plane (see Fig. 2). In the former situation, the wings align with the tether direction, making the wings-tether angle ζ equal to zero. In the latter, it is the aircraft's vertical axis e_Z that aligns with the tether direction, making the wings-tether angle ζ equal to 90 degrees. To overcome such a limitation, we have devised a bridle system with attachment points in both the wing and the fuselage surface, with a winch inside the aircraft (see Fig. 4). The actuation on the winch enables the bridle geometry, and thereby the wings-tether angle and roll angle, to be controlled. This control can be done for a wide range of values: for the wings-tether angle ζ between 0 and $\pi/2$ rad, corresponding to a roll angle ϕ between $\beta - \pi/2$ and β. This bridle system was developed in (Fontes et al., 2023) and we refer to it for further details.

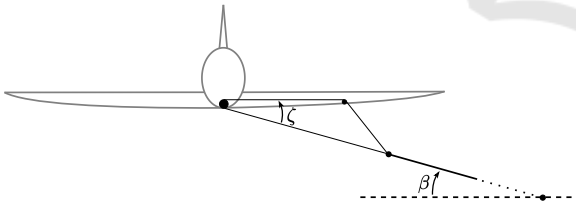

Figure 4: Bridle system with attachment points on both the wing and on the fuselage surface, with a winch inside the aircraft to change the bridle geometry and the wings-tether angle (in this figure, $\phi = 0$).

2.3 Coordinated Turn

The coordinated turn is a crucial flight condition in manned flight operations primarily for enhancing passenger comfort. It involves executing turns without experiencing lateral acceleration in the aircraft's body frame, resulting in a smoother flight experience. In our work, this technique allows the aircraft to execute turns instead of skidding laterally, thus reducing or even cancelling out the tension in the tether that is connected to the aircraft. If there is a situation in which the tether has to be released during the ATOL, this coordinated turn can be performed so that the aircraft can still perform the turn, without the tether. Otherwise, the instant release of the tether could result in instability or even a crash.

During a coordinated turn, the roll angle ϕ is set so that there is no net side force acting on the aircraft.

For this condition, the centrifugal force acting is equal and opposite to the horizontal component of the lift force. Moreover, in equilibrium, the vertical component of the lift force is equal and opposite to the vertical component of the gravity force. Summing the forces in the horizontal and vertical direction we have

$$F_{\mathrm{L}} \sin\phi = m\frac{(V\cos\gamma)^2}{R}, \tag{11}$$

$$F_{\mathrm{L}} \cos\phi = mg\cos\gamma, \tag{12}$$

where R is the curvature radius, the horizontal projection of the tether length r in the horizontal plane $R = r\cos\beta$. Dividing both equations we obtain the roll angle required for this maneuver

$$\tan\phi_{\mathrm{ref}} = \frac{V^2\cos\gamma}{gR}. \tag{13}$$

Since the wings-tether angle ζ is the variable that can be actuated directly via the bridle mechanism, we have

$$\zeta_{\mathrm{ref}} = \beta - \phi_{\mathrm{ref}} = \beta - \arctan\left(\frac{V^2\cos\gamma}{g\,r\cos\beta}\right). \tag{14}$$

2.4 Roll Controller

The roll control itself is an easy task since it is an immediate consequence of an actuated variable (recall $\phi = \beta - \zeta$). However by changing the roll, the vertical and horizontal components of the lift are modified, with consequences on the equilibrium of forces that the tethered aircraft is subject to. The challenge is then to maintain the equilibrium when changing the roll. Thus, we use a multivariable control method and as is usual in airplane control methodology, we devise a set of equilibrium points, compute a linearized model around those points, and design a Linear Quadractic Regulator (LQR) as the controller.

For the required values of β, α, γ and ϕ, we determine the equilibrium points with a speed V satisfying $(\dot{\beta}, \dot{V}, \dot{\gamma}, \dot{\theta}) = (0,0,0,0)$. In section 3, in Table 3, we report the values for the reference states used. The state considered to design the LQR does not include the azimuth angle φ. Since in CTOL we have an endless runway, there is no need to control the azimuth position φ. Moreover, the evolution of β, V_a, γ, and θ

described by the dynamic equations is not dependent on φ. As such, we can safely omit φ from the state-space considered for control purposes, just using it to draw the kite trajectories during the simulation.

In LQR, we start by defining the error state $\widetilde{\mathbf{x}} = \mathbf{X} - \mathbf{x}_{ref}$, and the error control $\widetilde{\mathbf{u}} = \mathbf{U} - \mathbf{u}_{ref}$. The linearized model around the equilibrium point $(\widetilde{\mathbf{x}}, \widetilde{\mathbf{u}}) = (0,0)$ is expressed as $\dot{\widetilde{\mathbf{x}}} = A\widetilde{\mathbf{x}} + B\widetilde{\mathbf{u}}$, where A and B are the Jacobian matrices computed at the equilibrium point.

The objective function $\int_0^\infty \left(\widetilde{\mathbf{x}}^T Q \widetilde{\mathbf{x}} + \widetilde{\mathbf{u}}^T R \widetilde{\mathbf{u}}\right) dt$, includes two matrices, Q and R, which are initially set to be diagonal and satifying the Bryson and Ho rule (Bryson and Ho, 1975). These matrices are then manually adjusted to achieve the desired response. Table 3 reports the values of the matrices used in the simulation for each phase.

In order to test the roll controllers, we devise an experiment with three loiter phases with different roll values (see Fig. 3).

In the first loiter phase, we maintain the wings-tether equal to zero (corresponding to roll angle equal to β). In the second loiter phase, we seek another simple control objective which is to attain zero roll, corresponding to leveled wings. In this case , we want that $\phi_{\text{ref}} = 0$ and $\zeta_{\text{ref}} = \beta$ These variables can be measured and controlled directly by the aircraft sensors and actuators (in our case using a small winch). In the third loiter phase, the control objective is to attain a coordinated turn. The variable to regulate is, as we have seen, the lateral acceleration a_Y. As the last case, this variable can be measured directly by the aircraft sensors.

The transitions between phases can be done by an operator command or after a specified time period. In this simulation, we defined as $t_{\text{loiter1}} \in [0,10]$s, $t_{\text{loiter2}} \in [10,30]$s and $t_{\text{loiterCT}} \in [30,60]$s to be the time in each loiter phase, respectively.

3 SIMULATION RESULTS

The simulation parameters were established considering a small-scale aircraft, facilitating the comparison of simulation results with future experiments data. The aircraft and simulation parameters are given in Table 2.

Table 2: Aircraft and Simulation Parameters.

$A = 0.0720\,\text{m}^2$, $m = 0.350\,\text{kg}$
$b = 0.60\,\text{m}$, $r = 30b = 18\,\text{m}$
$\omega_q \in [-20;20]^\circ\,\text{s}^{-1}$, $F_\text{p} \in [0;1.5]\,\text{N}$, $\zeta \in [0;90]^\circ$
$\rho = 1.225\,\text{kg}\,\text{m}^{-3}$, $g = 9.8\,\text{m}\,\text{s}^{-2}$, $V_w = 0\,\text{m}\,\text{s}^{-1}$

Table 3 provides a summary of the reference values and gains for the controllers tested for each phase. The controllers were implemented using Matlab/Simulink and the results of the simulation are displayed in Fig. 5.

Table 3: Controller references, gains, and objectives for each loiter phase.

Loiter with $\phi = \beta$
$(\beta, V, \gamma, \theta)_{ref} = (20.00, 8.95, 0, 0)$
$Q = \text{diag}([63.68\ \ 0.085\ \ 5.62e3\ \ 33.19])$
$R = \text{diag}([2.61\ \ 8.21])$
Loiter with $\phi = 0$
$(\beta, V, \gamma, \theta)_{ref} = (35.00, 10.57, 0, 0)$
$Q = \text{diag}([14.59\ \ 0.39\ \ 8.21\ \ 8.21])$
$R = \text{diag}([0.44\ \ 8.21\ \ 2.68])$
Coordinated Turn
$(\beta, V, \gamma, \theta)_{ref} = (50, 9.71, 0, 0)$
$Q = \text{diag}([14.59\ \ 0.39\ \ 8.21\ \ 8.21])$
$R = \text{diag}([0.44\ \ 8.21\ \ 2.68])$

In the left column of the figure, we can see the elevation angle of the kite on the left axis and the height on the right axis, on top of the velocity V of the aircraft. In the second column, we can see the pitch, angle-of-attack and flight-path angles on the top, and on the bottom the control variables: propeller thrust force and pitch rate (with different axes on the opposite side, respectively). Finally, in the right column, we can see the roll and wings-tether angles above the forces graph: tether force, the horizontal component of the lift force (F_L^h) and the inertial force magnitude. We can observe that the trajectories follow closely the references determined previously. Starting with the first loiter, where ζ is zero, the aircraft maintains its attitude and altitude/elevation for 10s without any changes. Then, in the second loiter phase, the roll angle is set to zero and the elevation angle to 35°. This makes the aircraft pitch up and accelerate until it reaches the new speed required for this new equilibrium point. As predicted, ζ goes to 35°, which equals the new elevation angle. Note that in this phase, the horizontal component of the lift force is zero, that is true when the roll is zero. Finally, after 20s in this second phase, the aircraft performs a coordinated turn flight with an elevation angle chosen as 50°. Here, the kite goes to a new equilibrium point where the wings-tether angle goes to the predefined value computed using equation (14), which is 10°. The new speed reference is also followed. We can also point out that in the coordinated turn phase, the tether force is zero,

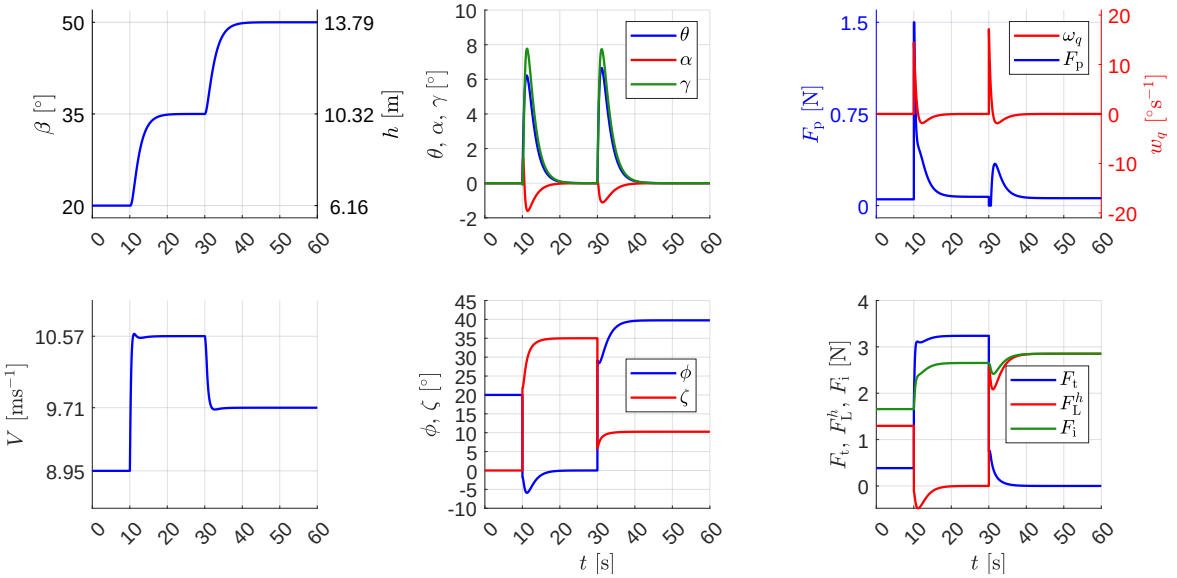

Figure 5: Simulation results during the 3 types of loiter.

which proves that if the tether needs to be released, the aircraft will still be able to perform the turn without it. Also, as predicted, the inertial force magnitude is equal to the horizontal component of the lift force acting on the aircraft.

4 DISCUSSION AND CONCLUSIONS

It was shown that the aircraft is able to successfully control its roll angle during each of the three phases described here. This paper, together with (Vinha et al., 2024b), reveals that the implementation of a circular take-off and landing approach, particularly for tethered aircraft like those employed in Airborne Wind Energy Systems, is viable and allows the automation required by this industry.

In the overall control architecture, we switch between different controllers. We are aware that such an approach might lead to instability issues. The simulation results do not show any unstable behavior. Nevertheless, the stability properties of the overall architecture should be studied in future work.

The tethered flight is here further explored by implementing a coordinated turn flight which grants the aircraft the capability to be released from its tether and remain stably airborne. However, a coordinated turn flight can only be performed within certain conditions. If we combine F_L from equations (11) and (7), and assuming that we are in a situation with $V_w = 0$, both V^2 terms can be cancelled. Also, if we assume that we are in the 1st loiter phase where $\zeta = 0$ and $\beta = \phi$, we can solve for β, obtaining:

$$\beta^* = \phi^* = \frac{1}{2}\arcsin\left(\frac{4m}{r\rho A c_L}\right), \quad \beta \in [0,45]^\circ. \quad (15)$$

This equation identifies, for the aircraft dimensions defined previously, the regions where it is possible to perform a coordinated turn flight for a specific tether length in this loiter phase. In Fig. 6, β^* is plotted for several tether lengths (dark line). This line corresponds to a situation in which the coordinated turn flight is performed with $\zeta = 0$ and the tether force is zero. A coordinated turn flight would be impossible to achieve for the flight conditions with the elevation and tether length in the red region (left and below the dark line). In this situation, the tether tension would be negative which is an impossible condition since the tether is not rigid.

Finally, the green area, above the dark line, is the region where any tethered flight can be achieved using a positive wings-tether angle. Here, the tether force is positive, partially canceling the centrifugal forces acting on the aircraft in this flight condition. Note that, in this region, the aircraft can also perform a coordinated turn flight, if the roll angle is set adequately. However, the use of a bridle device is essential to achieve such roll with a positive wings-tether angle, as was simulated in the third loiter case.

We can also conclude that the length of the tether serves as a crucial design parameter, significantly determining the maximum altitude achievable through a circular take-off and landing strategy, but also the conditions for which is possible to perform coordinated turn flights.

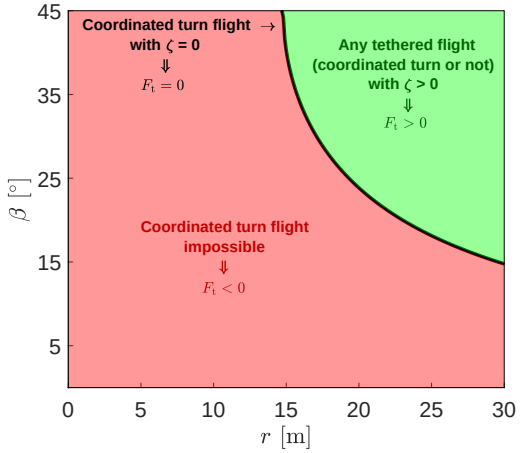

Figure 6: Plot of β^* for various tether lengths, using the aircraft parameters from the simulation.

ACKNOWLEDGEMENTS

This research is supported by FCT/MCTES (PIDDAC), through projects 2022.02320.PTDC-KEFCODE, and 2022.02801.PTDC-UPWIND-ATOL (https://doi.org/10.54499/2022.02801.PTDC), and grants 2021.06313.BD, and 2021.07346.BD.

REFERENCES

Beard, R. W. and McLain, T. W. (2012). *Small Unmanned Aircraft*. Princeton.

Blanch, M., Makris, A., and Valpy, B. (2022). Getting airborne – the need to realise the benefits of airborne wind energy for net zero. Technical report, Zenodo.

Bryson, A. E. and Ho, Y.-C. (1975). *Applied Optimal Control: Optimization, Estimation, and Control*. Taylor & Francis.

Cherubini, A. (2017). *Advances in airborne wind energy and wind drones*. PhD thesis, Scuola Superiore Sant'Anna.

Cherubini, A., Szalai, B., Schmehl, R., and Fontana, M. (2017). Preliminary Test on Automatic Take-Off and Landing of a Multi-Drone Low-Drag Airborne Wind Energy System. In *7th Airborne Wind Energy Conference (AWEC 2017)*.

Directorate-General for Research and Innovation (European Commission) and Ecorys (2018). *Study on challenges in the commercialisation of airborne wind energy systems*. Publications Office of the European Union, LU.

Fagiano, L. and Schnez, S. (2017). On the take-off of airborne wind energy systems based on rigid wings. *Renewable Energy*, 107:473–488.

Fernandes, G. M. (2023). Take-off and Landing of Autonomous Flying Wings in Airborne Wind Energy Systems. Master's thesis, Universidade do Porto, Porto, Portugal.

Fontes, F. A. C. C., Paiva, L. T., Fernandes, M. C. R. M., and Vinha, S. (2023). *A tethered aircraft bridle system, method of operating the same and use thereof*. Internal Report, SYSTEC, University of Porto.

Geebelen, K., Vukov, M., Zanon, M., Gros, S., Wagner, A., Diehl, M., Vandepitte, D., Swevers, J., and Ahmad, H. (2013). An Experimental Test Setup for Advanced Estimation and Control of an Airborne Wind Energy System. In Ahrens, U., Diehl, M., and Schmehl, R., editors, *Airborne Wind Energy*, Green Energy and Technology, pages 459–471. Springer, Berlin, Heidelberg.

Loyd, M. L. (1981). Wind driven apparatus for power generation.

Marques, M. N., Magalhães, S. A., Dos Santos, F. N., and Mendonça, H. S. (2023). Tethered Unmanned Aerial Vehicles—A Systematic Review. *Robotics*, 12(4):117. Number: 4 Publisher: Multidisciplinary Digital Publishing Institute.

Nguyen, H. T., Prodan, I., and Fontes, F. A. C. C. (2023). Trajectory Optimization and NMPC Tracking for a Fixed–Wing UAV in Deep Stall with Perch Landing. In *2023 European Control Conference (ECC)*, pages 1–7.

Rieck, B., Ranneberg, M., Candade, A., Bormann, A., and Skutnik, S. (2017). Comparison of Launching and Landing Approaches. In *7th Airborne Wind Energy Conference (AWEC 2017)*.

Riley, K., Hobson, M., and Bence, S. (2006). *Mathematical Methods for Physics and Engineering*. Cambridge University Press.

Schmehl, R., editor (2018). *Airborne Wind Energy: Advances in Technology Development and Research*. Green Energy and Technology. Springer, Singapore.

Sieberling, S., Ruiterkamp, R., de Bie, R., and Bontekoe, E. (2011). Discussion of a rotating platform for take-off and landing of a tethered aircraft. In *4th Airborne Wind Energy Conference (AWEC 2011)*.

Vermillion, C., Cobb, M., Fagiano, L., Leuthold, R., Diehl, M., Smith, R. S., Wood, T. A., Rapp, S., Schmehl, R., Olinger, D., and Demetriou, M. (2021). Electricity in the air: Insights from two decades of advanced control research and experimental flight testing of airborne wind energy systems. *Annual Reviews in Control*, 52:330–357.

Vinha, S., Fernandes, G. M., and Fontes, F. A. C. C. (2024a). A Discussion on Automatic Take-off and Landing Approaches for Airborne Wind Energy Systems. In *Book of Abstracts of the International Airborne Wind Energy Conference 2024*, Madrid, Spain.

Vinha, S., Fernandes, G. M., Nguyen, H. T., Fernandes, M. C., and Fontes, F. A. (2024b). Automatic Circular Take-off and Landing of Motorized Tethered Aircraft. In *2024 European Control Conference (ECC)*, pages 681–686.

Zanon, M., Gros, S., and Diehl, M. (2013). Rotational start-up of tethered airplanes based on nonlinear MPC and MHE. In *2013 European Control Conference (ECC)*, pages 1023–1028.